Initial results from a cryogenic proton irradiation of a p-channel CCD

Conference or Workshop Item

Initial Results from a Cryogenic Proton Irradiation of a p-channel CCD

J. P. D. Gow[a], D. Wood[a], D. Burt[b], D. J. Hall[a], B. Dryer[a], A. D. Holland[a] and N. J. Murray[a]
[a]Centre for Electronic Imaging, The Open University, DPS, Milton Keynes, MK7 6AA, UK
[b]e2v technologies plc, 106 Waterhouse Lane, Chelmsford, Essex, CM1 2QU, UK

ABSTRACT

The displacement damage hardness that can be achieved using p-channel charge coupled devices (CCD) was originally demonstrated in 1997 and since then a number of other studies have demonstrated an improved tolerance to radiation-induced CTI when compared to n-channel CCDs. A number of recent studies have also shown that the temperature history of the device after the irradiation impacts the performance of the detector, linked to the mobility of defects at different temperatures. This study describes the initial results from an e2v technologies p-channel CCD204 irradiated at 153 K with a 10 MeV equivalent proton fluences of 1.24×10^{9} and 1.24×10^{11} protons.cm^{-2}. The number of defects identified using trap pumping, dark current and cosmetic quality immediately after irradiation and over a period of 150 hours after the irradiation with the device held at 153 K and then after different periods of time at room temperature are described. The device also exhibited a flatband voltage shift of around 30 mV per krad, determined by the reduction in full well capacity.

Keywords: CCD, p-channel, cryogenic irradiation, proton radiation damage

1. INTRODUCTION

It is well known that the space radiation environment has a negative impact on the performance of the electronic systems within spacecraft through the damage caused by ionising and non-ionising radiation. In the case of optoelectronic devices the decrease in performance is caused by the creation of defects within the silicon bandgap, the impact on the operational performance is then dependant on the defect type, the sensor's operating conditions and also the sensor type. Lattice defects change the electrical properties of the silicon through a number of different processes, including generation (thermal generation of e-h pairs), recombination (charge is captured and is effectively lost) and trapping (charge is captured and released after some period of time)[1]. The impact of these defects is subject to the energy level created within the silicon bandgap, related to the type of impurity forming the defect, the speed at which charge is moving and the temperature of the silicon. Different detectors are more susceptible to certain types of defects, for example a charge coupled device (CCD) requires a number of charge transfers to read out, compared to the one transfer typically required by a complementary metal-oxide semiconductor image sensor (CIS), making the impact of trapping on charge transfer efficiency (CTE) of particular interest to those wishing to use a CCD in space.

It is possible through the selection of sensor type, including the material used for charge collection and transfer (n-channel or p-channel) and by performing a radiation damage mitigation study to select the optimal operating conditions for use in flight. Typically this has been performed at room temperature, however, based on the evidence from other studies looking into the performance of devices irradiated at cryogenic temperatures[2-11], this may not be sufficient for the latest precision astronomy missions where the location of even small amounts of charge needs to be accounted for. The aforementioned studies have shown that performing an irradiation at only room temperature can give misleading impressions of both the evolution of dark current, bright defects[2-5, 9-11] and CTE [2, 5-11]. These factors can have a large impact on the selection of the optimal operating conditions, and it is important not to fall into the trap of performing extensive optimisation based on the results of a room temperature study when the defects type and quantities that could impact the performance inflight, where the device is operating cryogenically, could be significantly different.

*jason.gow@open.ac.uk; phone +44 (0)1908 332194; fax +44 (0)1908 655667; www.open.ac.uk/cei

The study described in this paper is being performed as part of a European Space Agency (ESA) funded investigation into the performance benefits provided through the use of a p-channel rather than an n-channel CCD[12]. The full study includes a complete electro-optical characterisation of seven e2v technologies p-channel CCD204 devices and includes: optimal operational temperature, charge to voltage conversion factor, global and local photo-response non-uniformity, read out noise, non-linearity, image and register full well capacity, dark signal, dark signal non-uniformity, defects in darkness, charge injection uniformity, parallel and serial charge transfer efficiency, point spread function, modulation transfer function, quantum efficiency and trap identification by pumping. The overall aim to build upon our understanding of device behaviour, the benefits offered through the use of p-channel CCDs and also to provide inputs to modelling and simulation activities. The full study includes the irradiation of three p-channel CCD204 devices, where two irradiations were performed at room temperature and one with the device held at 153 K throughout the irradiation and for a period of 1 week after the irradiation. This was then followed by testing at 153 K interspaced by the device being held at room temperature for periods of 26 hours and 1 week and one month to assess the impact of holding the device at room temperature on its performance post irradiation.

This paper focuses on some of the early results from the cryogenic irradiation performed with the device operating normally at 153 K and the subsequent impact of the device being allowed to room temperature before cooling back to 153 K. The experimental arrangement and technique are described, followed by some of the initial observations of the dark current, bright defects and trap evolution post irradiation. The impact of flat-band voltage shift on the full well capacity of the device is also discussed, including a description of edge effects, something not observed during the irradiation of these devices when un-biased. The CTE performance is complicated by the changes in dark current and trap evolution and will be discussed in a future publication.

1.1 CCD204

The e2v technologies CCD204, shown in Figure 1, is manufactured on high resistivity bulk n-type silicon thinned to 70 μm (fully depleted). It is a 4k × 1k device with 12 μm square pixels, utilising a split register with two output nodes each of which can be operated using an amplifier responsivity of 4.5 μV/h$^+$ or 1.5 μV/h$^+$. It is based on the same architecture used in the CCD203, previously flown on board the Solar Dynamics Observatory launched in 2010[12], but with the inclusion of a charge injection structure. Both p-channel[13-14] and n-channel[15] variants have been produced.

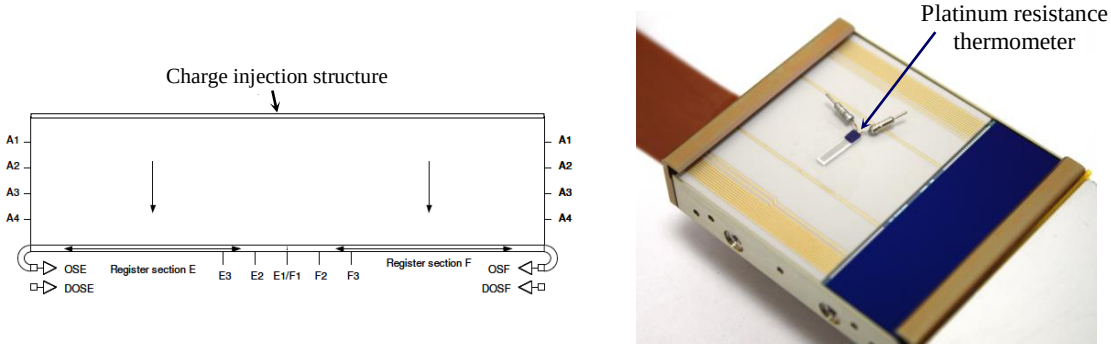

Figure 1. Schematic and photograph of the e2v technologies CCD204-22. The photograph shows the location of the platinum resistance thermometer (PRT) used to monitor the temperature of the device during data collection.

The serial register of the CCD204 is designed to allow on-chip pixel-signal binning to be possible, resulting in a channel width of 50 μm. The custom CCD273 developed for the Euclid visible imager[12, 16] is based on the CCD204 but, as binning is not required, with a register width of 20 μm to provide an improvement in serial CTE, as has been measured using Mn-Kα X-rays giving a factor of around 1.7[17], the same principle could be applied to the p-channel CCD204 in future variants.

2. EXPERIMENTAL ARRANGEMENT

During the irradiation, performed using 7.5 MeV protons from the Synergy Health 5MV Tandem accelerator (UK), and the data collection, the device under test was held in a modified Centre for Electronic Imaging (CEI) vacuum test facility, shown in Figure 2 mounted on the end of the proton beamline. The CCD under test was clamped onto a copper cold bench connected to a CryoTiger® refrigeration system capable of cooling the CCD to around 140 K. The temperature was controlled using a feedback system, comprising a Lakeshore 325 temperature controller, platinum resistance thermometer (PRT), and a heater. An XTF5011/75-TH X-ray tube was used to fluoresce a polished manganese target held at 45° to the incident X-ray beam to provide around one X-ray event per eighty pixels. Flat field illumination, the non-uniformity being within 5% across the device, was provided by two light emitting diodes (LED) placed at the far end of the chamber. Clocking and biasing were provided by an XCAM ltd. USB2REM2 camera drive box in conjunction with drive software controlled use a custom MatLab software program.

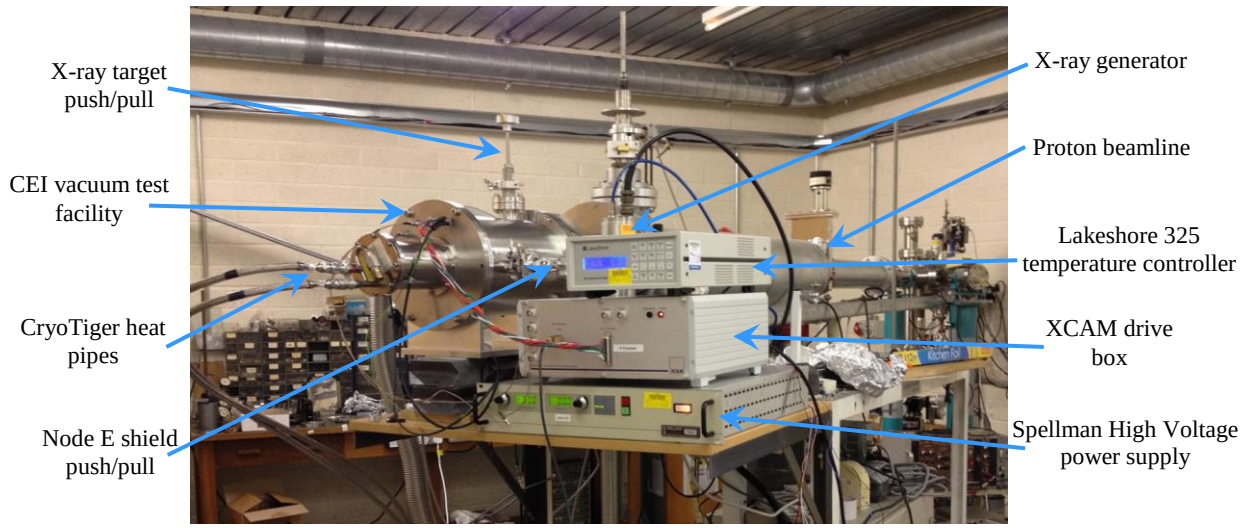

Figure 2. Photograph of the CEI vacuum chamber attached to the end of the Synergy Health proton beamline.

During the irradiation the X-ray target was raised out of the beam using the push-pull labelled in Figure 2. The 10 mm thick aluminium proton shields, shown in Figure 3, were attached to rotational push pulls to enable to shields to be moved into, Figure 3(a), and out of the beam, Figure 3(b), thereby allowing the two nodes to be irradiated with a different fluence. A shield guide was mounted around the device, indicated in Figure 3, to ensure that the shields, held 3 mm from the surface of the CCD, could move easily without risk of hitting the surface of the CCD. Rotational push pulls were used both to allow a slight rotation to be applied to hold the shields in place during data collection, shown in Figure 3(b), but also to allow four different regions to be irradiated for a future application of the test equipment where a larger 4k x 4k CCD273 will be irradiated. The headboard, which contains the pre-amplifiers for the two output nodes, was also shielded during the irradiation.

During data collection a gate valve was closed to isolate the test chamber from the beamline, this was included to allow the test chamber to be removed while keeping the device at 153 K and also to isolate it from the beamline which contains a number of viewing ports. These ports were covered with aluminium foil during the irradiation, however it is likely that there would still be light leakage making data collection without isolating the chamber un-advisable.

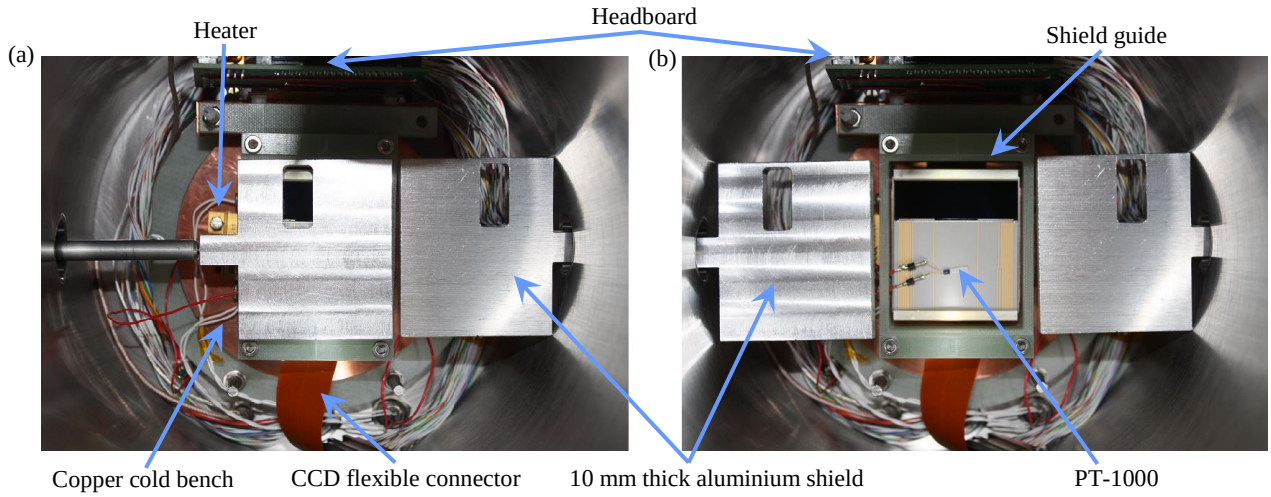

Figure 3. Aluminium shields in position to irradiate node F (a) and withdrawn (b) for data collection.

2.1 Proton Irradiation

The proton irradiation was performed utilising three p-channel CCD204s using 7.5 MeV protons from the Synergy Health 5MV Tandem accelerator (UK). The area irradiated on each device is shown in Figure 3(a). This region of irradiation was selected to provide an on chip control, i.e. the region next to the output node was left un-irradiated, while still allowing an assessment of parallel and serial CTE to be performed. Details on the flux and 10 MeV equivalent fluence delivered to each device is given in Table 1.

Device	Details	Image Region	7.5 MeV proton fluence (protons.cm^{-2})	7.5 MeV flux (protons.cm^{-2})	10 MeV equivalent proton fluence (protons.cm^{-2})
10092-06-02	Control	AE	Control Device		
		AF			
10092-04-03	Room Temp	AE	3.07×10^{9}	2.1×10^{7}	4.0×10^{9}
		AF	1.53×10^{9}	1.8×10^{7}	2.0×10^{9}
10092-01-04	Room Temp	AE	7.66×10^{10}	1.5×10^{7}	1.0×10^{11}
		AF	1.23×10^{10}	1.6×10^{7}	1.6×10^{10}
10092-04-05	Cryogenic	AE	7.66×10^{10}	3.4×10^{7}	1.0×10^{11}
		AF	7.65×10^{8}	3.5×10^{7}	1.0×10^{9}

Table 2. Proton irradiation details for the room temperature and cryogenic irradiation

During the cryogenic irradiation the CCD was biased and acquiring images, but the majority of the images collected during the irradiation were saturated in signal, with the exception of the lucky image shown in Figure 4. The start of the image acquisition period occurred after the proton beam had been turned off, so the beam was being powered down as charge was being clocked through the device prior to the start of a 10 s integration.

The image clearly shows the area of the device that was unshielded, it also shows a decreasing amount of charged particle interaction outside of the shielded region. Based on previous irradiations the interaction of protons on the edge of the shielded region was evident by an increased dark current on the edge of the irradiation area, due to protons loosing energy within the shield and then causing increased amounts of damage to the detector. It is interesting to note how far across the device protons still interact. It should be noted that the flux in the shielded region will be many orders of magnitudes less than the direct irradiation and values recorded in the control region are comparable to pre-irradiation levels. The irradiated region also indicates a number of charged particle interactions after the beam was powered down;

these are the result of material being activated during the irradiation and the subsequent short lived decay process. The increase in dark current can also be observed, and shows the area that received direct irradiation.

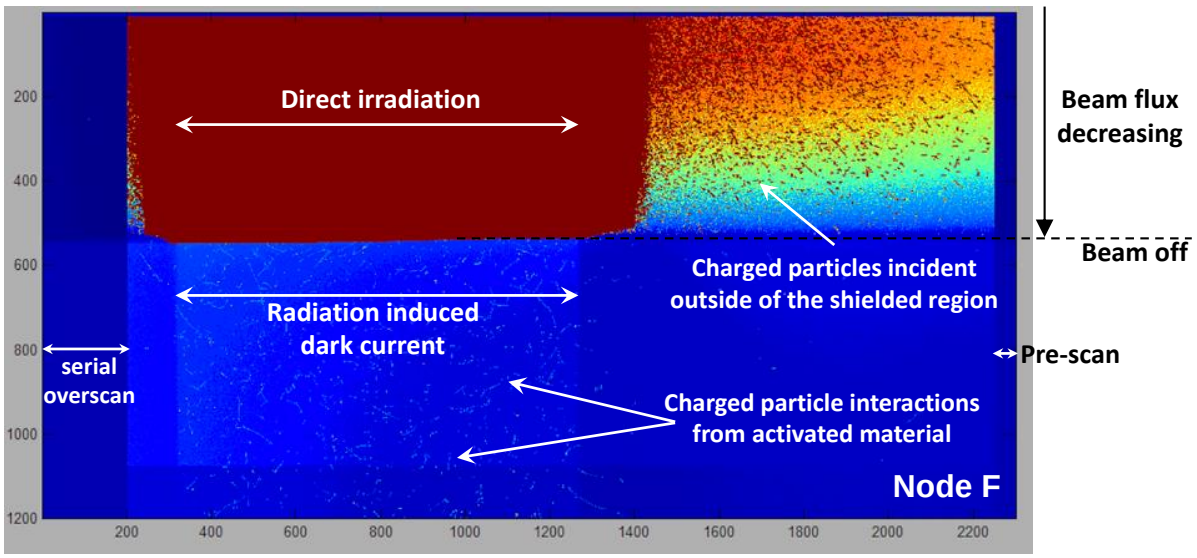

Figure 4. A lucky image taken as the beam was powered down during the last irradiation. The direct irradiation of the area under the shield, protons scattering within the shield incident in the shielded region, radioactive decays from activated material and the impact of radiation induced dark current can all be observed.

3. EXPERIMENTAL TECHNIQUE

The CCD204 was typically readout at 50 kHz using a parallel transfer pulse time (toi) of 1,000 µs, but the read-out speed was increased to 100 kHz during the collection of trap pumping data to enable more images to be collected in a reduced period of time. The dark current and number of bright defects were determined using three images taken with an integration time of 360 s. A bright defect was defined as a pixel exhibiting greater than 50 and 200 holes with the surrounding eight pixels being below a threshold of 100 holes, this requirement should be met in three images for the identification of a bright defect to be made. The full well capacity was assessed by reading out the device with the LEDs emitting continuously to provide an increasing amount of charge within the detector as a function of row number, with an additional pause inserted after the serial line transfer to ensure the full well of the device was exceeded. The full well was defined as the point where the non-linearity exceeded 3% and referred to Sat_{Lin}, and is the point at which the potential under the collecting phase is comparable to that of the barrier phase thereby resulting in charge blooming.

The trap pumping analysis relies on moving the charge backwards and forwards in the parallel direction using the clocking shown in Figure 5. The intensity of the resulting dipole is dependent on the phase time, t_{ph}, increasing to the point at which the trap has maximum effect is most efficient and then decreasing as the t_{ph} is increase further, as shown in figures 6 and 7 which show the dipole intensity as a function of t_{ph} for the divancancy and carbon interstitial defects respectively. It should be noted that these plots were recorded prior to the irradiation, indicating the presence of both types of defects within the un-irradiated silicon. The emission time constant of the trap can then be calculated by fitting

$$Dipole\ Amplitude = NP_C\left(exp\left(\frac{-t_{ph}}{\tau_e}\right) - exp\left(\frac{-2t_{ph}}{\tau_e}\right)\right) \quad (1)$$

where N is the number of pumping cycles (in this study 4,000), P_C is the probability of capture and τ_e is the emission time constant, to the data in figures 6 and 7. The resulting fit to the data is shown in both figures, further information on this method can be found in Hall *et al*[18].

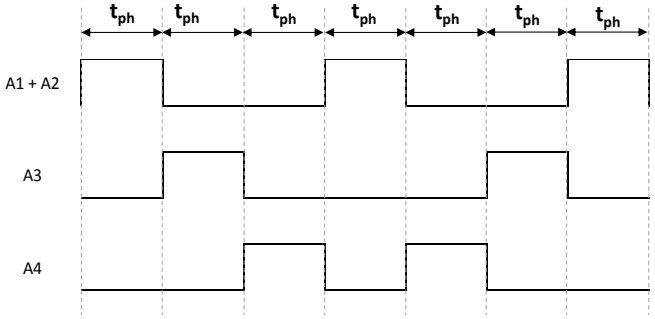

Figure 5. Clocking scheme used during trap pumping analysis, the phase time, t_{ph}, is varied to identify individual traps emission time constants

This process, depending on the emission time constant of the trap being investigated, requires many hours to provide the number of data points shown in figures 6 and 7. To investigate the defect behaviour post irradiation, this had to be reduced and two different methods were considered. The first was to operate the device using only a t_{ph} equivalent to the peak amplitude for the two traps that could be investigated, the carbon interstitial and the divancancy. The second was to select key points along the profile and use those to determine the trap type. The issue with the first method is that it relies on the assumption that if a trap is identified using that value of t_{ph}, then it is precisely the trap that is being looked for. This could however result in erroneous identification should other trap species with similar emission time constants be detected, but it does allow for increased time resolution. The second method increases the accuracy of the identification and allows, to a limited extent when compared to extensive data collection, one to determine subtleties in trap emission time constants while only requiring tens of minutes to complete a full trap sweep. The trap sweeping method was therefore selected for this study, the points used to identify the carbon interstitial and divancancy defects are shown in figures 6 and 7 respectively.

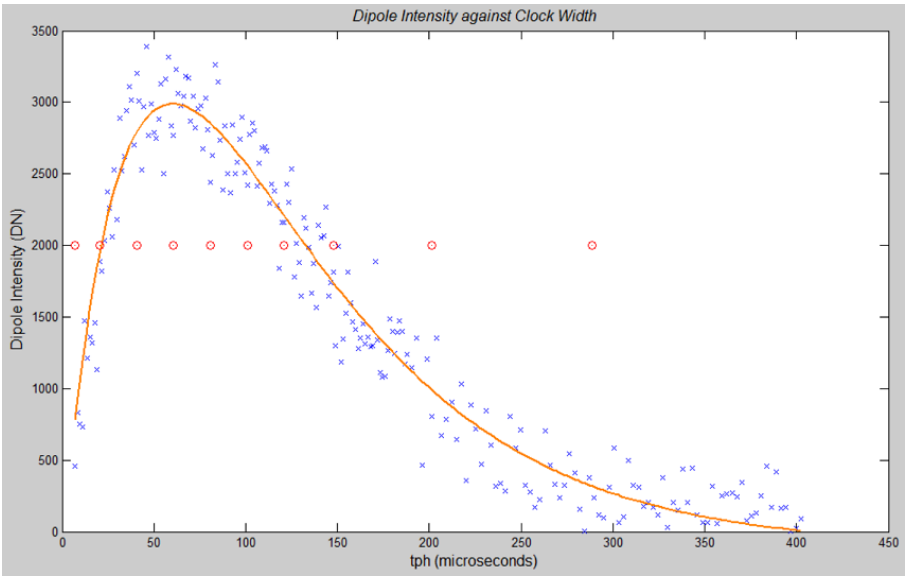

Figure 6. Dipole intensity as a function of t_{ph} showing a divancancy defect measured pre-irradiation, the points selected to enable the trap to be quickly identified are indicated by the red circles

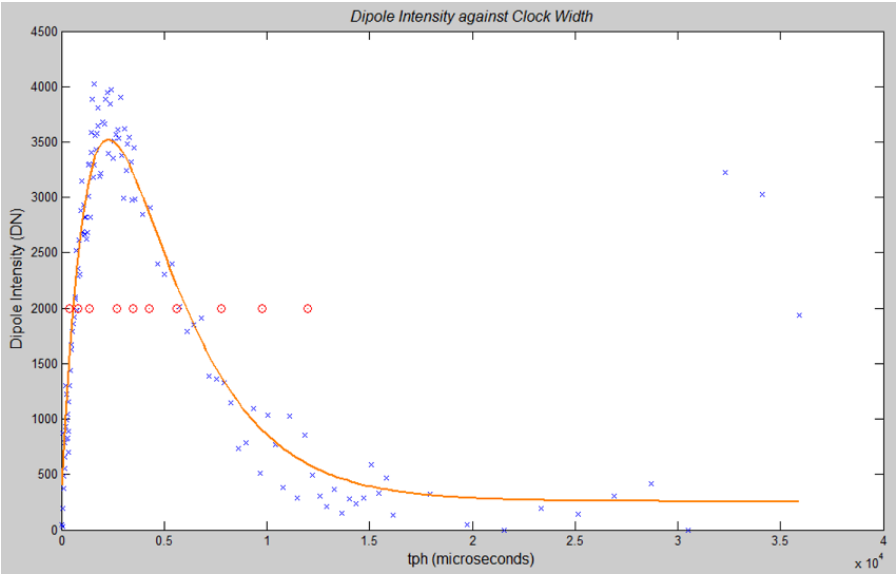

Figure 7. Dipole intensity as a function of t_{ph} showing a carbon interstitial defect measured pre-irradiation, the points selected to enable the trap to be quickly identified are indicated by the red circles

4. RESULTS AND DISCUSSIONS

The dark current measured within the device after the irradiation as a function of temperature is shown in Figure 8; the point at which the various irradiations finished and the periods that the device was at room temperature are also indicated. What is evident is that there is a significant increase in dark current after the irradiation, followed by a gradual reduction which, even after 153 hours was still reducing, at a considerable slower rate than immediately after the initial irradiation. After a period at room temperature there is an 80% decrease in the dark current followed by a continued reduction and, upon being held at room temperature for a further week, the dark current remained within error. Unfortunately the device was operated at different temperatures as part of the main study which meant not as much data could be collected at 153 K post 26 hours at room temperature.

The observed trend in dark current is similar to previously reported behaviour[5], including the second dip after the first period at room temperature. The other irradiated region follows a similar trend. The control regions also exhibit an increase in the dark current recorded; this could be as a result of residual charge left within the serial register after the transfer because the serial register dump function was not used after the completion of each successive read-out. Another possibility is that it is the impact of deep traps which captured charge during the irradiation and are slowly emitting over an extended period of time. It is likely that inflight operation under continual radiation bombardment will be similar to the performance just prior to the device being brought to room temperature for the first time.

The number of bright defects above 50 and 200 holes (after 360 s) created in node E irradiated with a 10 MeV equivalent proton fluence of 1.24×10^{11} protons.cm^{-2} is shown in Figure 9. As with the dark current there is a rapid decrease immediately after the irradiation, with values appearing to level out just prior to the device being allowed up to room temperature. After the device was held at room temperature, only one bright defect could be identified using the same criteria. Only a few bright defects were created in node F.

The image taken to determine the change in full well capacity using node E irradiated with a 10 MeV equivalent proton fluence of 1.24×10^{11} protons.cm^{-2} is shown in Figure 10. The onset of blooming occurs around 300 rows earlier than in the control region, and indicates a decrease in the Sat_{Lin} of around 50k holes. The reduction in full well is likely to be the resulting flatband voltage which occurs during the irradiation, in e2v n-channel CCDs this is typically between 0.1 and 0.2 V per krad for a standard gate and 6 mV per krad for thin gate with the device biased during the irradiation. The total ionising dose (TID) delivered during the irradiation was 64.7 krad. Assuming the voltage shift is linear and using pre-irradiation data from device 10092-04-03 where the full well was measured as a function of clock voltage, the initial

estimate of the flatband voltage shift was found to be around 30 mV per krad. The Sat_{Lin} full well capacity of the irradiated device will be measured as a function of image clock voltage to confirm the relationship and provide an updated estimation of the flat-band voltage shift. The likely cause of the reduced flatband shift in the p-channel CCD when compared to an n-channel device is the result of the formation of trapped holes in the oxide being compensation by electrons trapped in the Si_3N_4 (of the Si_3N_4-SiO_2 gate dielectric), thereby resulting in a lower flatband shift[19].

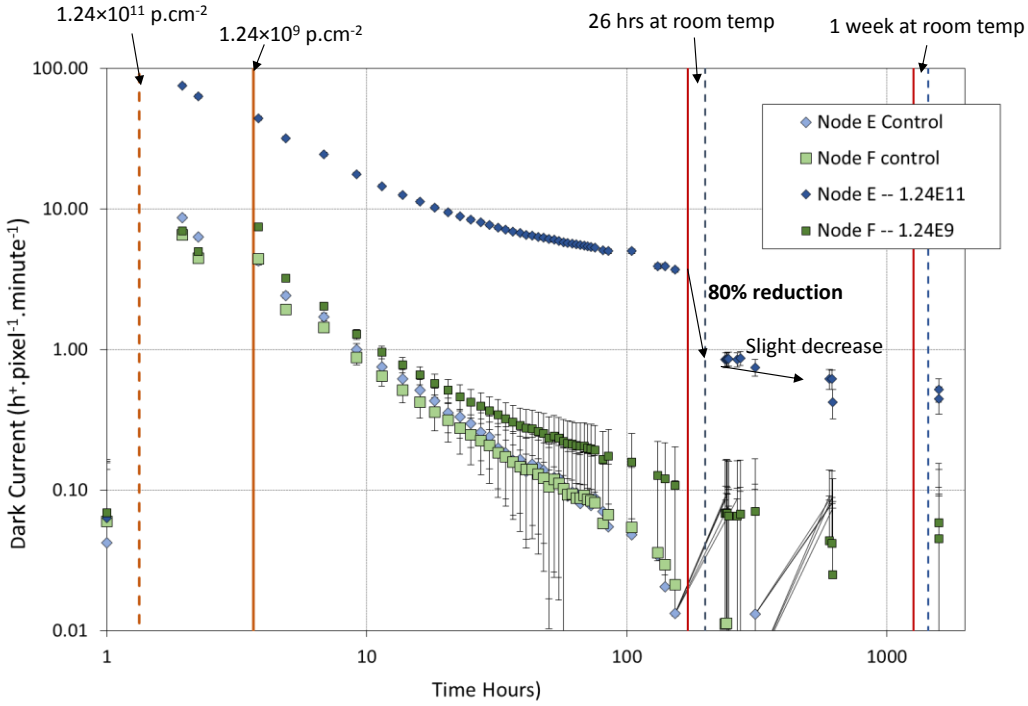

Figure 8. Dark current as a function of time in the two irradiated regions and their respective control regions

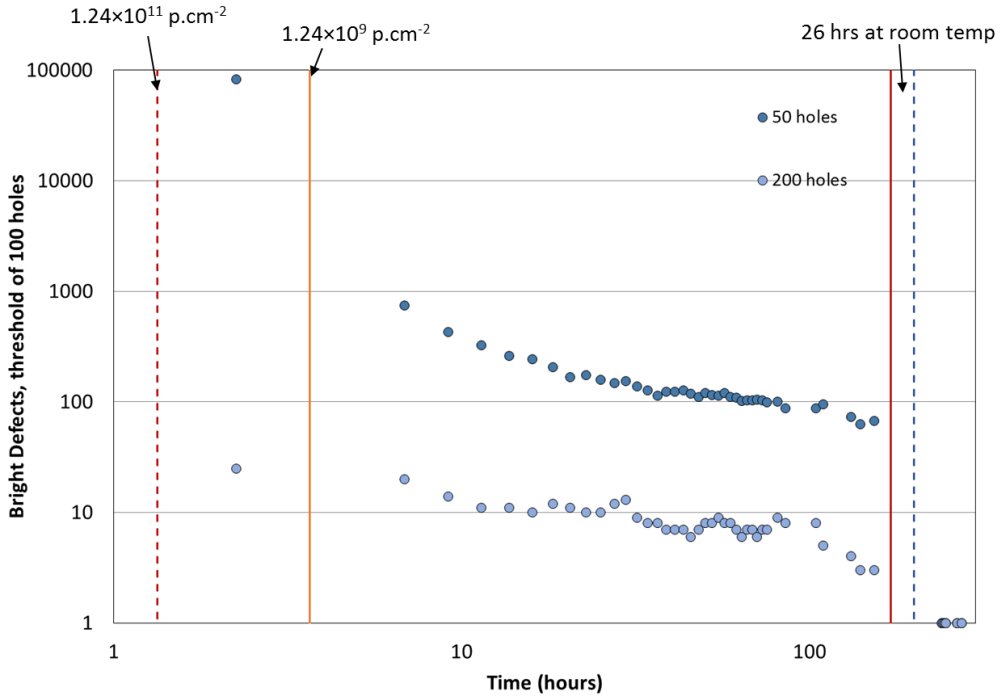

Figure 9. Number of bright defects as a function of time in the region irradiated with a 10 MeV equivalent proton fluence of 1.24×10^{11} protons.cm^{-2}

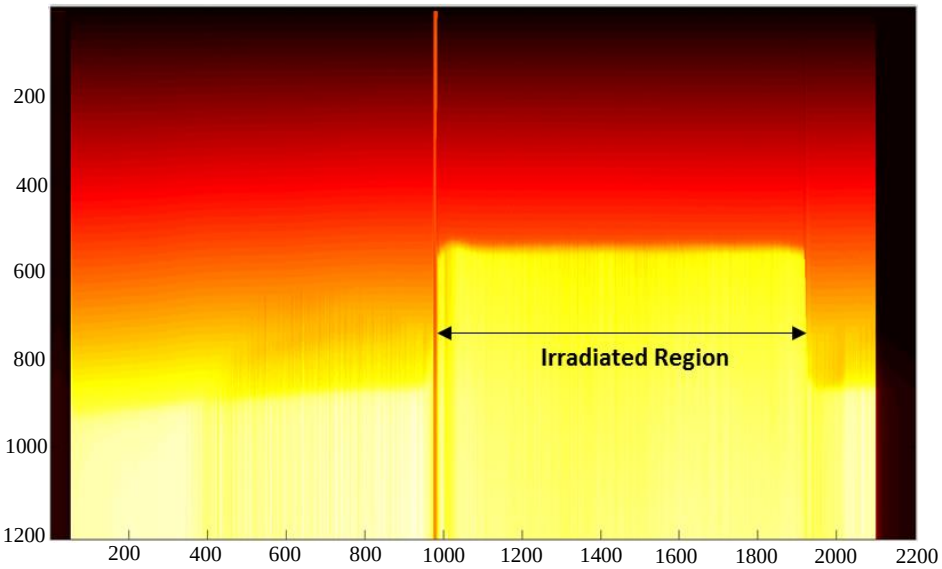

Figure 10. Image resulting from an LED being powered on while the device is read out. The reduction in full well capacity in the region irradiated with a 10 MeV equivalent fluence of 1.24×10^{11} protons.cm^{-2} is evident by the step change increase in signal as the device becomes saturated in that region

The other interesting phenomenon that can be observed in Figure 10 are the two bands which mark the edge of the irradiated region of the device; a close up image is shown in Figure 11 taken using a uniform flat field exposure of 20k holes. The same effect cannot be observed in node F and the bands are not observed in a device which was irradiated at room temperature and un-biased to a comparable proton fluence. The cause of this effect is likely to do with the preferential movement of charge towards a region of increased potential resulting in the redistribution of charge and the formation of light and dark bands at the edge of the irradiated region, a cartoon illustration of the process is shown in Figure 12. The process is the same as that which occurs during point spread function measurements commonly referred to as the bright fatter effect[20], however in this case the description of charge redistribution[21] is more appropriate.

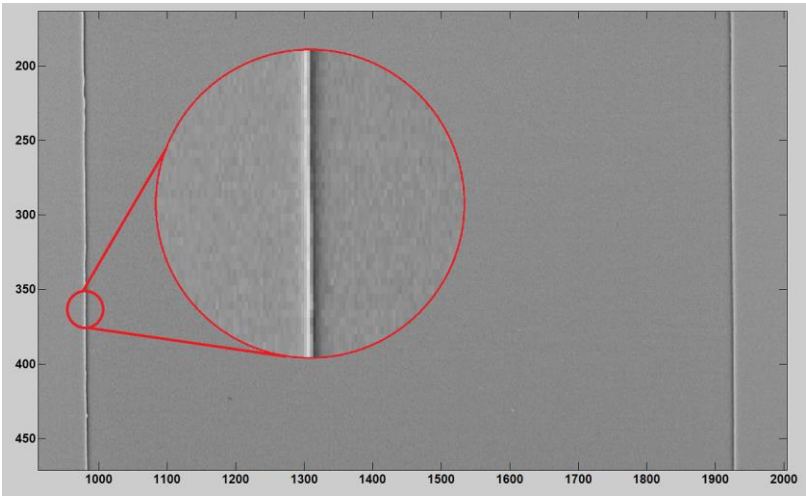

Figure 11. Image taken using a flat field exposure of 20,000 holes, cropped to show the area irradiated with a 10 MeV equivalent fluence of 1.24×10^{11} protons.cm^{-2} and the charge redistribution which occurs on the boundaries of the irradiation

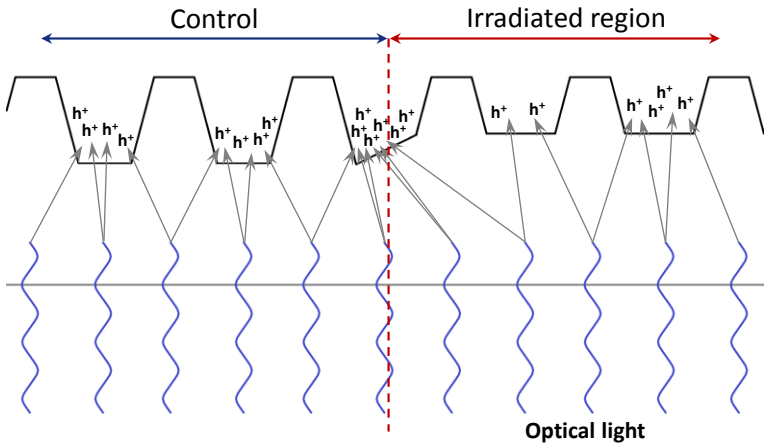

Figure 12. Simplification of the process which occurs at the edges of the irradiation where charge preferentially moves towards regions with the greatest potential

The number of defects identified in a region of 239k pixels as a function of time after the irradiation is shown in Figure 13 for the divancancy and Figure 14 for the carbon interstitial. In both cases there is an increase in the number of defects after the irradiation, followed by a gradual reduction as the device remained at 153 K. Data was collected closer to the end of the irradiation using the trap sweeping method. However the presence of charged particle interaction requires more in-depth analysis to ensure the correct number of traps can be determined. The increase in the number of traps after the irradiation was confirmed by looking at trap-pumping images taken as soon as the kit could be accessed after the irradiation was complete, shown in Figure 15. The number of traps is in the same region of the device is shown prior to the irradiation, Figure 15(a), 6 minutes after the irradiation, Figure 15(b), and 18 minutes after, Figure 15(c), with a differenced image, Figure 15(d), showing the increase in number of traps over the period of 12 minutes. After the device was held at room temperature the number of divancancy defects has increased by around a factor of 9. It should be noted that although the divancancy is not mobile at this temperature, the vacancy is. The number of carbon interstitial defects has decreased by around 50% after 26 hours at room temperature. The carbon interstitial is mobile at room temperature and is therefore able to form other stable defects. A more detailed analysis of the data is currently underway, looking at the behaviour of individual traps and the impact on their emission time constants after the period at room temperature; this will form part of a future publication once the analysis has been completed.

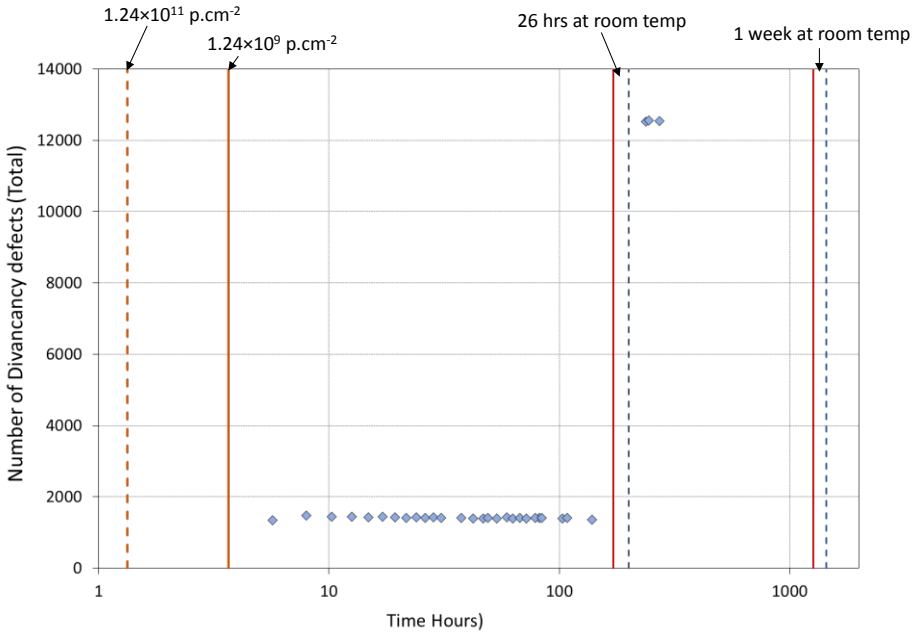

Figure 13. Number of divancancy defects recorded after the irradiation as a function of time

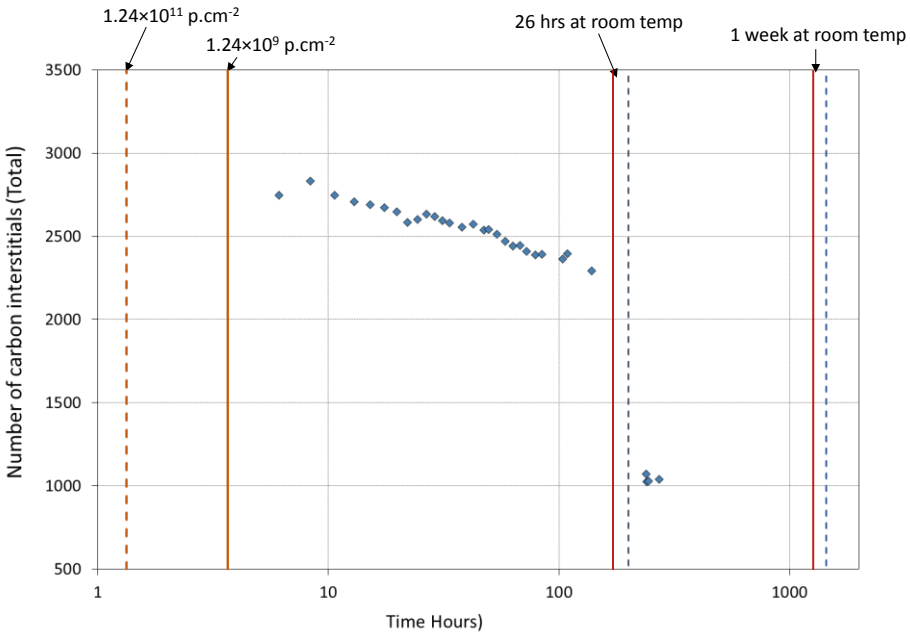

Figure 14. Number of carbon interstitial defects recorded after the irradiation as a function of time

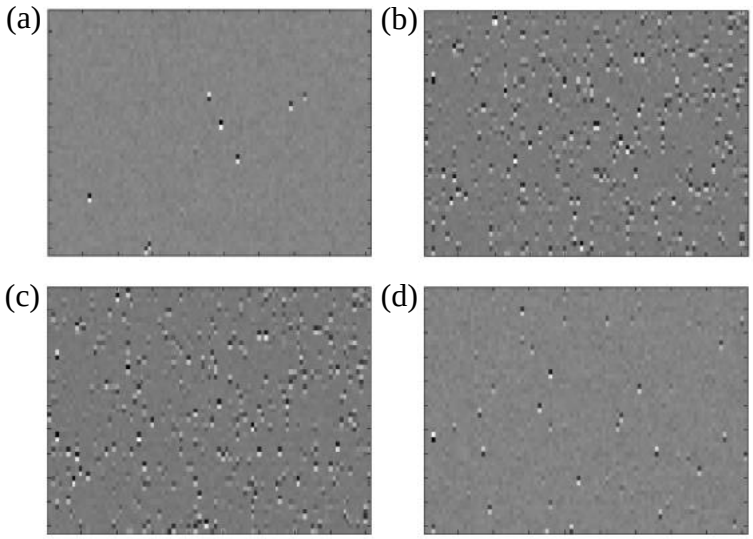

Figure 15. Image showing the results of trap pumping in a section of the device pre-irradiation (a), 6 minutes after the irradiation was complete (b), 18 minutes after the irradiation was complete (c) and a difference image (d) showing the change over a period of 12 minutes

5. CONCLUSIONS

The behaviour of a number of parameters is highly dynamic immediately post irradiation and monitoring everything is challenging and it could be advisable in a future irradiation to focus primarily on one parameter with occasional monitoring of other parameters. Both the dark current and the number of bright defects exhibit a rapid decline post irradiation and even after 150 hours have not yet stabilised. It is likely that in-flight performance would be similar to the performance at which stabilisation occurs. However, before this can be confirmed, it would be advisable to perform irradiations at different flux rates and monitor the performance until the parameter of interest have stabilised.

Although the nature of p-channel silicon means that the full well capacity of the device is reduced with incident ionising radiation, it has been shown the flatband voltage shift, calculated to be 30 mV per krad, is significantly less than in a standard gate n-channel CCD. This makes p-channel devices suitable for use in high total ionising dose environments. The identification of preferential charge redistribution is also of interest, although in normal operation it is unlikely that such a step change in dose across the device would be incurred so as to make it an issue for inflight operation.

The evolution of the two defects explored as part of this study is extremely interesting and provides a window into the behaviour of individual defects as they are both formed and anneal over periods of time, both with the device held at 153 K and also after a period of time spent at room temperature. A significant quantity of data have been collected to allow a more detailed investigation into this behaviour to be performed and will form party of a future publication.

The impact on the CTE of both the changing dark current and number of trapping defects makes the analysis of CTE more complicated than previous radiation campaigns where data collection was performed under stable operating conditions, i.e. fixed dark current and trap numbers. Therefore further analysis of the CTE is required and will be described in a future publication.

Data continue to be collected with the cryogenically irradiated device after increasing periods at room temperature and the data collection and analysis of the room temperature irradiated devices will also be completed in the near future allowing a comparison of the two data sets and with previously irradiated n-channel CCDs to be performed. It would also be advisable to continue to monitor the device performance over an extended period of time, i.e. years to identify possible continued changes in performance. The equipment and methodologies developed as part of this study have already been utilised in an n-channel cryogenic irradiation study that is currently ongoing. The equipment will also be used, and slightly modified, for a planned future n-channel CCD irradiation which will include a 'keep cold and return' irradiation where the device will be transported back to the CEI for monitoring over an extended period of time (years).

It is likely that with the continued development of precision astronomy missions, performing an optimisation of the operating speeds and temperature after the device has been irradiated cryogenically will be highly recommended. The temperature aspect requires a study to confirm if the same performance is achieved if the device is irradiated at one temperature to if it is irradiated colder and then allowed to warm to that temperature.

REFERENCES

[1] Srour J. R., Marshall C.J., and Marshall P.W., "Review of Displacement Damage Effects in Silicon Devices," IEEE Trans. Nucl. Sci. 50(3), (2003).

[2] Kimble R. A., Goudfrootij P., and Gilliland R. L., "Radiation damage effects on the CCD detector of the space telescope imaging spectrometer," Proc. SPIE 4013, (2000).

[3] Polidan E. J., Waczynski A., Marshall P. W., *et al.*, "Hot pixel behavior in WFC3 CCD detectors irradiated under operational conditions," Proc. SPIE 5167, (2004).

[4] Marshall C. J., Marshall P. W., Waczynski A., *et al*., "Hot Pixel Annealing Behavior in CCDs Irradiated at -84 °C," IEEE Trans. Nucl. Sci. 52(6), (2005).

[5] Dawson K., Bebek C., Emes J., *et al*., "Radiation Tolerance of Fully-Depleted P-Channel CCDs Designed for the SNAP Satellite," IEEE Trans. Nucl. Sci. 55(3), (2008).

[6] Bautz M., Prigozhin G., Kissel S., *et al*., "Anomalous Annealing of a High-Resistivity CCD Irradiated at Low Temperature," IEEE Trans. Nucl. Sci. 52(2), (2005).

[7] Grant C. E., LaMarr B., Prigozhin G. Y., *et al*., "Physics of reverse annealing in high-resistivity Chandra ACIS CCDs," Proc. SPIE 7021, (2008).

[8] Hopkinson G., Short A., Vetel C., *et al*., "Radiation Effects on Astrometric CCDs at Low Operating Temperatures," IEEE Trans. Nucl. Sci. 52(6), 2664-2671 (2005).

[9] Hopkinson G., and Mohammadzadeh A., "CCD Radiation Testing at Low Temperatures Using a Laboratory Alpha Particle Source," IEEE Trans. Nucl. Sci. 53(6), (2006).

[10] Hopkinson G. R., Gare P., and Sarri G., "Effects of Low Temperature Proton Irradiation on a Large Area CCD for Astrometric Applications," IEEE Trans. Nucl. Sci. 57(4), (2010).

[11] Gow J. P. D., Smith P. H., Pool, P., *et al*., "Proton Irradiation of a CCD236 Swept Charge Device at Cryogenic Temperature and the Subsequent Annealing," JINST 10 C01037, (2015).

[12] Endicott J., Darby S., Bowring S., *et al*., "Charge-Coupled Devices for the ESA Euclid M-class Mission," Proc. SPIE 8453, (2012).

[13] Murray N. J., Holland A. D., Gow J. P. D., *et al*., "Assessment of the performance and radiation damage effects under cryogenic temperatures of a P-channel CCD204s," Proc. SPIE 9154, (2014).

[14] Gow J. P. D., Murray N., Holland, A. and Burt, D., "Proton damage comparison of an e2v technologies n-channel and p-channel CCD204," IEEE Trans. Nucl. Sci., 61(4), 1843–1848 (2014).

[15] Gow J. P. D., Murray N., Holland, A., *et al*., "Assessment of space proton radiation-induced charge transfer inefficiency in the CCD204 for the Euclid space observatory," JINST 7 C01030, (2012).

[16] Cropper M., Pottinger S., Niemi S., *et al*., "VIS: the visible imager for Euclid," Proc. SPIE 91430J, (2014).

[17] Gow J. P. D., Murray N. J., Hall, D. J., *et al*., "Assessment of proton radiation-induced charge transfer inefficiency in the CCD273 detector for the Euclid Dark Energy Mission," SPIE Article 845316, (2012).

[18] Hall D. J., Murray N. J., Holland A. D., *et al*., "Determination of in situ trap properties in CCDs using a "single-trap pumping technique," IEEE Trans. Nucl. Sci. 61(4), 1826–1833 (2014).

[19] Saks N.S., Killiany J.M., Reid P.R., and Baker W.D., "A radiation hard MNOS CCD for low temperature applications," IEEE Trans. Nucl. Sci. 26(6), 5074–5079 (1979).

[20] Antilogus P., Astier, P. Doherty P., *et al*., "The brighter-fatter effect and pixel correlations in CCD sensors," JINST 9 C03048, (2014).

[21] Edgar A., Murray N., Stefanov K., *et al*., "Point-spread function and photon transfer of a CCD for space-based astronomy," Proc. SPIE 8860, (2013).